Computational-Fluid-Dynamics-Based Evaluation and Optimization of an Entrained-Flow Gasifier Potential for Coal Hydrogasification

ARTICLE *in* ENERGY & FUELS · OCTOBER 2013

Impact Factor: 2.79 · DOI: 10.1021/ef4013032

6 AUTHORS, INCLUDING:

He Boshu
Beijing Jiaotong University
52 PUBLICATIONS **249** CITATIONS
SEE PROFILE

Zhipeng Duan
Beijing Jiaotong University
42 PUBLICATIONS **347** CITATIONS
SEE PROFILE

energy&fuels

Article

pubs.acs.org/EF

Computational-Fluid-Dynamics-Based Evaluation and Optimization of an Entrained-Flow Gasifier Potential for Coal Hydrogasification

Linbo Yan, Boshu He,* Xiaohui Pei, Chaojun Wang, Huaxin Liang, and Zhipeng Duan

School of Mechanical, Electronic and Control Engineering, Beijing Jiaotong University, Beijing 100044, People's Republic of China

ABSTRACT: To evaluate and optimize a developed two-stage entrained flow bed gasifier when it is used for the coal hydrogasification (CHG) process, a series of comprehensive three-dimensional numerical simulations designed with the orthogonal method are carried out. The effects of different operating conditions, including the reaction pressure p, H_2/coal mass ratio $R_{h/c}$, and O_2/H_2 mass ratio $R_{o/h}$ on the fields and the evolution histories of the gasification parameters as well as the carbon conversion rate (CCR), the CH_4 mole fraction (MMF), and the cold gas efficiency (CGE) are analyzed, and meaningful conclusions are obtained. The hydrogasifier proposed in this work performs well. Counter flow can be detected in the gasifier and is beneficial for char conversion. The gas temperature and MMF increase with the height of the gasifier, while the hydrogen mole fraction (HMF) decreases. The water mole fraction (WMF) increases with the height of the gasifier if the gasification temperature is high; otherwise, it will decreases slightly. The distribution of CH_4 in the top zone of the reductor tends to be homogeneous with the increase of $R_{o/h}$. Ranked in descending order, the effect degrees of the operating conditions on CCR, MMF, and CGE are $R_{o/h} > p > R_{h/c}$, $p > R_{h/c} > R_{o/h}$, and $R_{h/c} > R_{o/h} = p$, respectively. The optimum combinations of the operating conditions for CCR, MMF, and CGE are p = 7 MPa, $R_{h/c}$ = 0.7, and $R_{o/h}$ = 1.5; p = 7 MPa, $R_{h/c}$ = 0.3, and $R_{o/h}$ = 1.5; and p = 3 MPa (p = 5 MPa), $R_{h/c}$ = 0.7, and $R_{o/h}$ = 1.25, respectively. After comprehensive analyses, a synthetically optimal combination of the operating condition is proposed. With this condition, CCR can reach 96.78%, MMF can reach 17.42%, and CGE can reach 76.4%.

1. INTRODUCTION

Coal gasification technology has had more than 200 years of history,[1,2] and it is the basis for many clean coal utilization technologies, such as the integrated gasification combined cycle (IGCC)[3] and the zero emission coal (ZEC) systems.[4−6] There are lots of coal gasification technological processes, such as Texaco, E-Gas, Shell, Prenflo, etc.[2] There are also many kinds of coal gasifiers, such as the fixed bed, fluidized bed, entrained-flow bed, etc. The products of coal gasification are also various, e.g., syngas, hydrogen, liquid fuel, etc. Entrained-flow-bed gasifiers have been widely developed and used over the years, and they are usually used for the coal or biomass gasification with oxygen and/or steam.[7] As mentioned in our former work,[8] hydrogasification of coal is a relatively new technology and has attracted much attention for its unique advantages. Many experiments[9−11] on coal hydrogasification (CHG) have been performed, and even some semi-industrial hydrogasifiers[12,13] have been developed. However, almost all of the hydrogasifiers used in the lab-scale or the semi-industry experiments have a cylindrical shape. The simple structure is very proper for the validation of the hydrogasification mechanism, but whether it is proper for the practical industry production is still doubtful. Therefore, it is worth studying the characteristics of different types of gasifiers when they are used for CHG. In this work, an entrained-flow-bed gasifier, which is originally designed for coal gasification with oxygen, is exploited to serve as the hydrogasifier and the corresponding characteristics are assessed.[14−16] This gasifier is chosen because it has been successfully used in the IGCC system; therefore, it is expected that the gasification technology can also be used in the ZEC system, which is similar to the IGCC system. However, this two-stage gasifier has not been used for coal hydrogasification before; thus, the inlet conditions (the flow rate and composition of the gasification agent, the flow rate of coal, and the allocation of the gasification agent among the nozzles) of the gasifier should be designed first. When the proper range of the operating conditions are found, nine sets of cases with different boundary conditions are then designed with the orthogonal method and the corresponding numerical simulations are carried out. Through this research, the following CHG properties of this gasifier are investigated. First, the fields of the main gasification parameters are drawn and analyzed to understand the gasification properties on the whole. Then, the evolutions of the main gasification parameters along the height of the gasifier are detected to further understand the gasification process in the gasifier. Third, the sensitivities of the carbon conversion rate (CCR) defined by eq 1, the CH_4 mole fraction (MMF), and the cold gas efficiency (CGE) defined by eq 2 to the different operating conditions, including the reaction pressure p, H_2/coal mass ratio $R_{h/c}$, O_2/H_2 mass ratio $R_{o/h}$, are studied using the orthogonal analysis method. The optimum combinations of the operating conditions for CCR, MMF, and CGE are also obtained. Finally, on the basis of the comprehensive analyses, a synthetically optimum combination of the operating conditions for the whole CHG is proposed

$$\mathrm{CCR} = 1 - \frac{C_{\mathrm{left}}}{C_{\mathrm{input}}} \tag{1}$$

Received: July 10, 2013
Revised: October 16, 2013
Published: October 16, 2013

   dx.doi.org/10.1021/ef4013032 | *Energy Fuels* 2013, 27, 6397−6407

where C_{left} denotes the mass of the unreacted carbon from the gasifier and C_{input} denotes the total mass of carbon in the coal fed to the gasifier

$$\mathrm{CGE} = \frac{G_{\mathrm{HHV}}}{F_{\mathrm{HHV}}} \quad (2)$$

where G_{HHV} denotes the total released high heating value of the cooled syngas from the gasifier and F_{HHV} denotes the total high heating value of the inlet fuel (H_2 and coal in the present work).

The schematic diagram of the pilot-scale gasifier is shown in Figure 1. It is a 200 tons/day up-flow gasifier tested in Japan

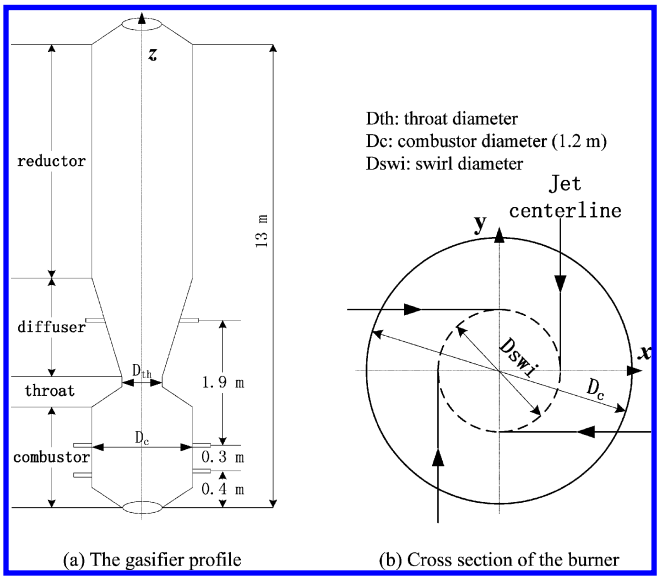

Figure 1. Schematic diagram of the gasifier.

and consists of a combustor, a diffuser, and a reductor. The combustor and diffuser are separated by a throat. The gasifier is originally developed for coal gasification with air. Parts of coal and the recycled char are burned with oxygen in the combustor cavity to supply the heat required and the gasification agent. The left coal is then injected into the reductor, where the gasification reactions take place. The design parameters of the gasifier are listed in Table 1, where the swirl ratio (SR) is defined as the ratio of the diameter of the circle formed by the tangential injection centerlines (D_{swi}) to the combustor diameter (D_c).

Table 1. Furnace Design Parameters[15]

ratio of D_{th}/D_c	SR of the lower combustor injector	SR of the higher combustor injector	SR of the reductor injector
0.4	0.5	0.63	0

2. CASE DESCRIPTION

2.1. Case Design. As mentioned above, in the original gasifier, parts of air and coal are injected into the combustor and burned to generate the hot gasification agent (CO_2). Then, the remaining parts of air and coal are injected into the reductor through the four nozzles assembled on the diffuser wall, and the gasification proceeds. Imitating the two-stage technology, O_2 and excessive H_2 are injected into the combustor and burned to generate the gasification agent (H_2 and H_2O) and the heat in the present work. Then, feed coal is injected into the reductor with N_2 and the surplus H_2, and the hydrogasification proceeds. The dominant reactions in the hydrogasifier are listed in Table 2. The kinetic correlations for the heterogeneous and

Table 2. Dominant Reactions in the Hydrogasifier

heterogeneous reactions	$C(s)+2H_2 \rightarrow CH_4$	(R1)
	$C(s)+CO_2 \rightarrow 2CO$	(R2)
	$C(s)+H_2O \rightarrow CO + H_2$	(R3)
homogeneous reactions	$CO + H_2O \rightarrow CO_2 + H_2$	(R4)
	$CH_4 + H_2O(g) \rightarrow CO + 3H_2$	(R5)
	$C_6H_6 + 6H_2O(g) \rightarrow 6CO + 9H_2$	(R6)
	$C_6H_6 + 8H_2 \rightarrow 4CH_4 + C_2H_6$	(R7)
	$C_2H_6 + 2H_2O(g) \rightarrow 2CO + 5H_2$	(R8)
	$H_2 + 0.5O_2 \rightarrow H_2O$	(R9)

homogeneous reactions can be found in our former work.[8] The kinetic correlation for R9 can be found in ref 17. Because this two-stage gasifier has not been used for coal hydrogasification before, the inlet conditions (the flow rate and composition of the gasification agent, the flow rate of coal, and the allocation of the gasification agent among the nozzles) of the gasifier need to be designed first. It is hard work to find out the proper inlet conditions, especially when the effect of gravity is considered for the quite complex flow field in the gasifier. When the flow rate of the gasification agent is large, the particle residence time will be very short, which is adverse to the carbon conversion rate. When the flow rate is small, the coal particles will drop down to the bottom of the combustor because of gravity. When the particle injection velocity is high, the particles will concentrate in the center area of the gasifier. When the particle injection velocity is low, the particles will concentrate in the near-wall area because of the centrifugal force. Thus, many pioneer simulations need to be performed to find out the proper range of the hydrogasification boundary conditions. When the proper range is known, nine cases with different combinations of p, $R_{h/c}$, and $R_{o/h}$ are designed using the orthogonal method, as listed in Table 3, to study the effects of different

Table 3. Orthogonal Table

case number	p (MPa)	$R_{h/c}$	$R_{o/h}$
1	3	0.3	1
2	3	0.5	1.25
3	3	0.7	1.5
4	5	0.3	1.25
5	5	0.5	1.5
6	5	0.7	1
7	7	0.3	1.5
8	7	0.5	1
9	7	0.7	1.25

operating conditions (p, $R_{h/c}$, and $R_{o/h}$) on the gasification results, especially on CCR, MMF, and CGE. There are in total three factors, and each factor has three levels; thus, the L_9 (3^4)-type orthogonal table is chosen. $R_{o/h}$ is defined as the mass ratio of the inlet O_2 to the inlet H_2. $R_{h/c}$ is defined as the mass ratio of the residue H_2 after burning to the inlet coal. From Table 3, it can be seen that the gasification pressure is set as 3, 5, and 7 MPa. This is because the coal hydrogasification requires high-pressure conditions to promote the carbon conversion rate. However, when the reaction pressure is too high, it will not be economical for the industry production. This range of pressures is the most typical; therefore, it is chosen in this work. The hydrogen/coal mass ratio, $R_{h/c}$, is set as 0.3, 0.5, and 0.7. This is because the theoretical mass ratio of H_2/C of the char methanation reaction, R1, is 1:3. Thus, the lower limit of $R_{h/c}$ is set as 0.3. If $R_{h/c}$ is too high, the gasification products can be strongly diluted by H_2. The

dx.doi.org/10.1021/ef4013032 | Energy Fuels 2013, 27, 6397−6407

Table 4. Analyses of Coal Used in This Work

approximate analysis				ultimate analysis				
M_{ad}	V_{ad}	C_{ad}	A_{ad}	C	H	O	N	S
1.95	39.11	50.66	8.28	81.45	5.57	7.94	1.68	3.36

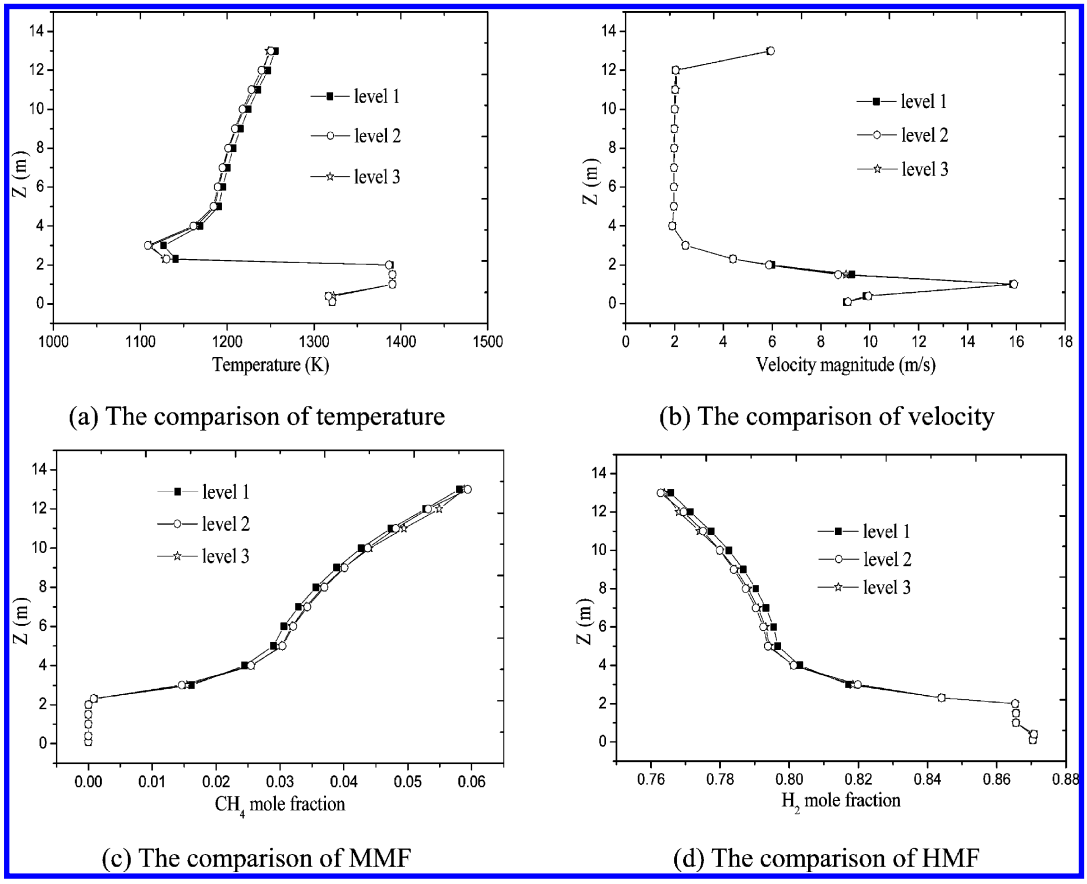

Figure 2. Comparisons of parameters along the height of the gasifier.

oxygen/hydrogen mass ratio, $R_{o/h}$, is set as 1, 1.25, and 1.5. This is because, when $R_{o/h}$ is lower than 1, the temperature of the gasification agent will be low and it is diverse to the gasification process. However, when $R_{o/h}$ is too high, the temperature of the gasification agent will be very high and the content of H_2O in the gasification agent will be high enough too. In this case, the gasification product will mainly be CO rather than CH_4. The Kentucky No. 9 high volatile coal is used in this work, and the analysis of this type of bituminous coal is listed in Table 4. All of the walls of the gasifier are considered as an adiabatic boundary in this work for the convenience of comparison.

2.2. Numerical Methods. The realizable $k-\varepsilon$ (RKE) model[18] is incorporated to calculate the turbulence in the gasifier where strong swirl velocity or counter flow occurs. The discrete phase model (DPM) is used to model the gas−solid flow in the entrained-flow-bed gasifier. The discrete ordinates (DO) radiation model, which allows for particle radiation and is applicable in a wide range of optical thicknesses, is used to model the gas−solid flow radiation.[19] The adsorption coefficient of the gaseous mixture is calculated with the weighted-sum-of-gray-gases model (WSGGM).[20] The eddy-dissipation concept (EDC) is used to calculate the turbulent reaction.[21] The combined random pore and shrinking core model with pressure correction (CRPSC−PC) developed in our former work[8] is used to predict the char heterogeneous reaction process. The *in situ* adaptive tabulation (ISAT) method, which can greatly reduce the time consumed by the chemical reaction calculations in multidimensional flow simulations, is used.[22] To restrain the numerical diffusion, the governing equations are discretized by the QUICK difference scheme and solved with the SIMPLEC algorithm. To make the simulations more time-efficient and easier to converge, a simulation strategy of the gas-phase cold-flow simulation followed by the gas−solid-phase hot-flow simulation is implemented. The effect of gravity on the particle motion is also considered in this work.

2.3. Independence of the Grid. Before the whole set of cases are simulated, the independence of the grid is checked. The block meshing concept is used so that the whole calculation domain can be partitioned with hexahedral cells. With the boundary conditions of case 1 as listed in Table 3, simulation results from three levels of meshes, including 34 911 (grid A), 54 216 (grid B), and 85 401 (grid C) hexahedral cells, are compared. The comparisons of the area-weighted-average values of velocity magnitude, temperature, MMF, and H_2 mole fraction (HMF) at different heights along the z direction are shown in panels a−d of Figure 2, respectively. The comparisons of the CCR and the particle residence time (PRT) among the three levels of meshes are listed in Table 5.

Simulation results shown in Figure 2 from the three mesh levels are very close to each other, especially those with grids B and C. From

Table 5. CCR and PRT Obtained from the Three Levels of Meshes

	grid A	grid B	grid C
CCR	14.43	12.49	12.54
PRT	9.25	8.52	8.59

dx.doi.org/10.1021/ef4013032 | *Energy Fuels* 2013, 27, 6397−6407

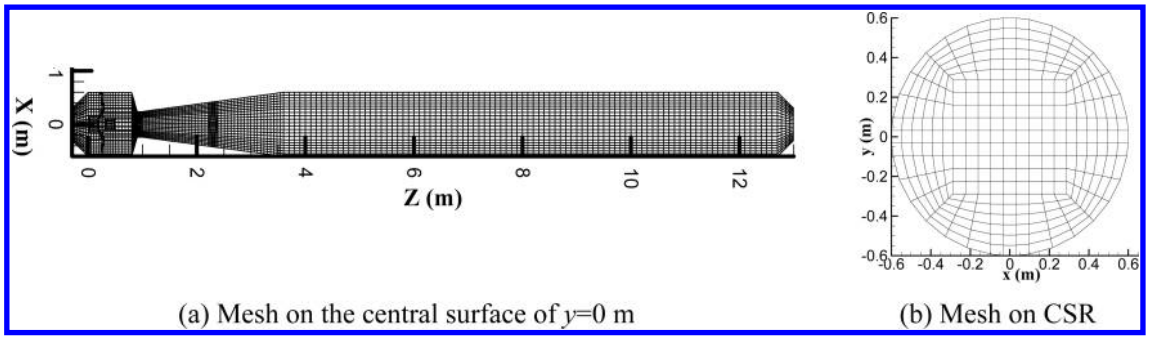

Figure 3. Mesh partition for the two-stage entrained-flow gasifier.

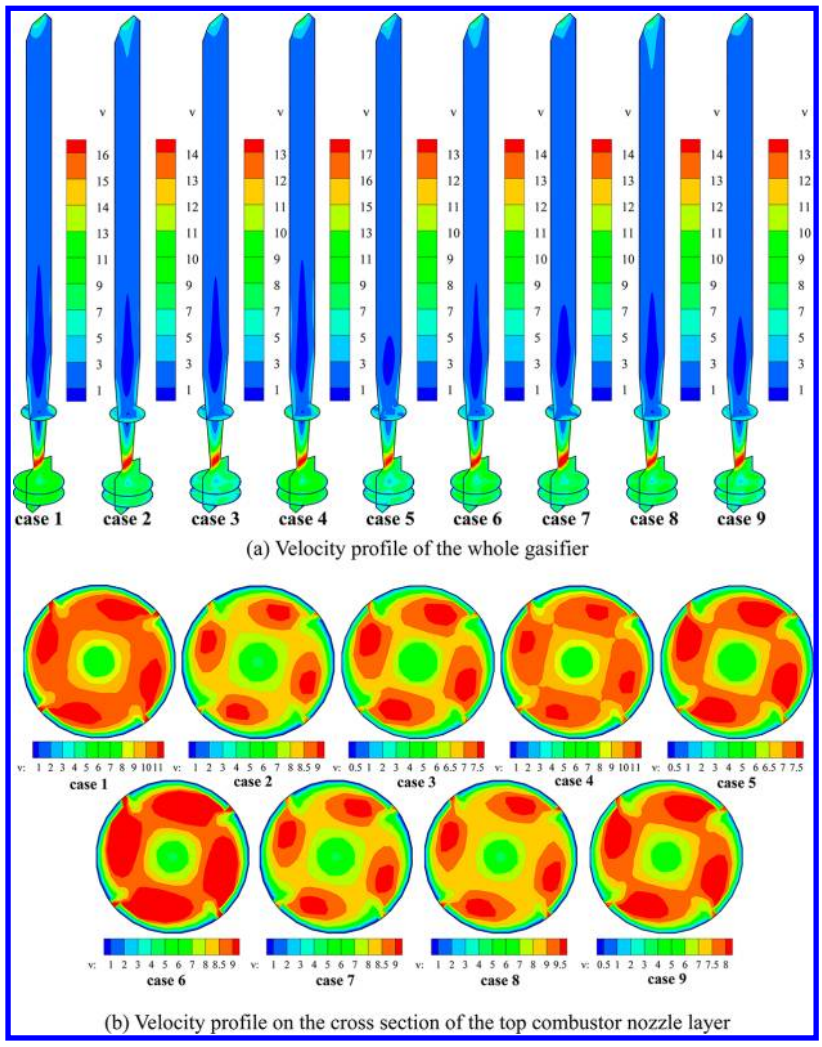

Figure 4. Velocity magnitude contours for cases 1−9.

Table 5, it can be seen that CCR and PRT calculated with grids B and C agree with each other very well. Thus, grid B with 54 216 hexahedral cells is justified to generate the grid-independent results and is chosen to do the following simulations. The meshes on the central surface (y = 0 m) of the gasifier and the cross-section of the reductor (CSR) are depicted in Figure 3.

3. SIMULATION RESULTS

3.1. Field Analyses. To detect the distribution of the flow field in the gasifier, the contour maps of different reacting flow parameters of the nine cases are drawn and compared. The velocity magnitude (v) contours, temperature (temp) contours, O_2 mole fraction (OMF) contours, CH_4 mole fraction (MMF) contours, H_2O mole fraction (WMF) contours, and H_2 mole fraction (HMF) contours on the central surface of the gasifier of the nine cases are depicted in Figures 4−9, respectively.

From Figure 4, it can be seen that the gas flow field of the nine cases are similar to each other. Figure 4a shows that counter flow is generated in the central area at the top of the diffuser zone, which is due to the swirl flow generated by the tangential injections from the combustor burner nozzles, as depicted in Figure 4b. The counter flow can extend the particle residence time to a certain extent and is beneficial to the coal conversion. The gas velocity is relatively high when it flows

dx.doi.org/10.1021/ef4013032 | *Energy Fuels* 2013, 27, 6397−6407

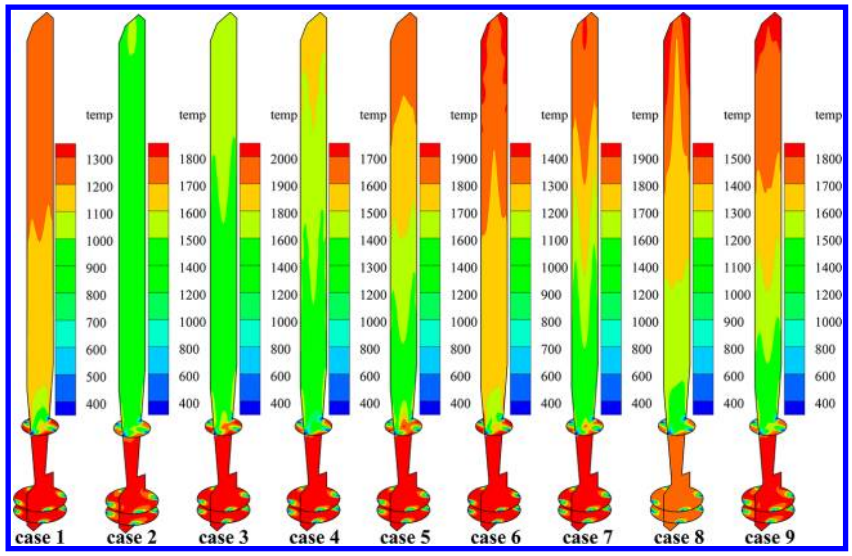

Figure 5. Temperature contours for cases 1−9.

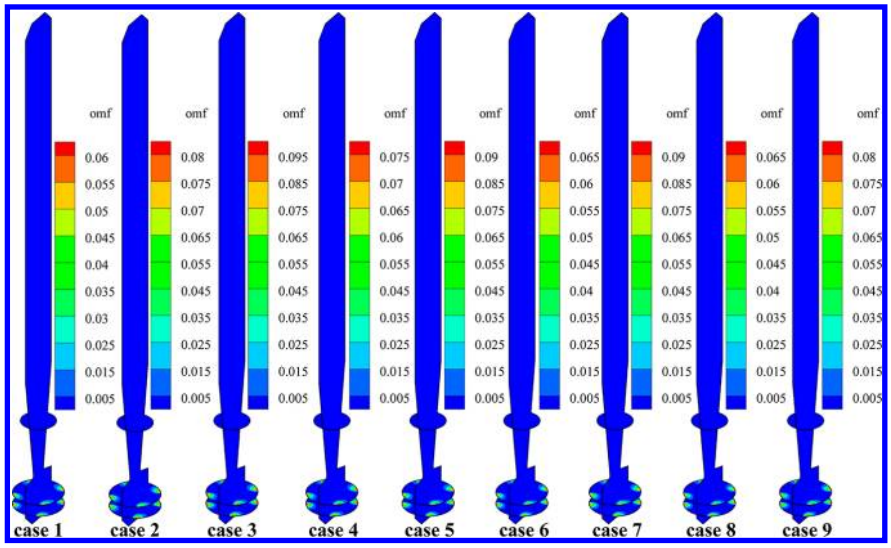

Figure 6. OMF contours for cases 1−9.

through the throat, which will prevent the unreacted coal particles in the diffuser and the reductor from dropping down to the bottom of the combustor and keep the hydrogasification process in the reductor. Velocity field is the base of the gasification process and can directly affect the gasification results. If the flow velocity is too low, the coal particle will drop down to the combustor. If the flow velocity is too high, on the other hand, the coal particle will escape from the gasifier quickly. Both of the two cases are adverse to the coal gasification. In addition, the swirl velocity in the gasifier can generate a centrifugal force for the coal particles. If the swirling intensity is high enough, the coal particles will concentrate in the near-wall area; otherwise, the coal particles will concentrate in the central area of the reductor. The principle of constructing the gas flow dynamic field in the gasifier in this work is to make the particle residence time as long as possible on the premise that the particles form an entrained-flow bed by controlling the gas flow rate. Moreover, the distribution of the coal particles in the gasifier is controlled by the swirl intensity and the particle injection velocity. It can also be seen from Figure 4 that the velocity fields are almost symmetric. This is because the geometric shape of the gasifier and the boundary conditions are all symmetric.

Referring to Table 3, Figure 5 shows that the general temperature distribution in the gasifier is mainly dependent upon $R_{o/h}$. When $R_{o/h}$ is high, the gas temperature in the gasifier will be high. For example, $R_{o/h}$ in case 3 is 1.5 and the corresponding peak temperature is about 2000 K, while $R_{o/h}$ in case 1 is 1 and the corresponding peak temperature is only about 1300 K. In the diffuser zone, when the hot gasification agent mixes with the cold coal and the cold N_2 and H_2 injected from the diffuser nozzles, the gas mixture temperature drops sharply. Then, the gas temperature increases gradually with the hydrogasification process. This is because the coal hydrogasification reaction, R1, is the dominant reaction and is exothermic. The temperature has a great impact on the chemical reaction kinetics. When the reaction temperature is high, the reaction rate will be fast. When the reaction temperature is low, however, the reaction rate will be slow. Because every reaction occurs along with heat generation or absorption, the reaction temperature then will have an apparent effect on the equilibrium of the reaction. Because R1 is

dx.doi.org/10.1021/ef4013032 | *Energy Fuels* 2013, 27, 6397−6407

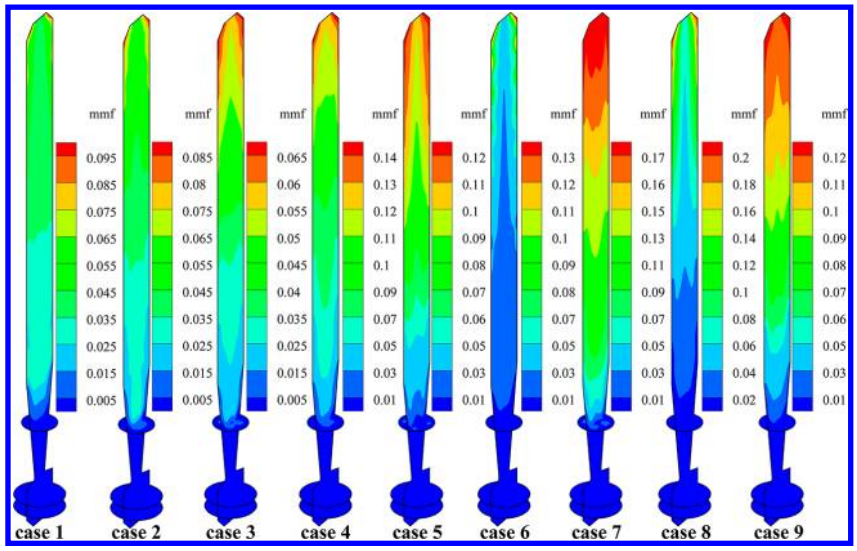

Figure 7. MMF contours for cases 1−9.

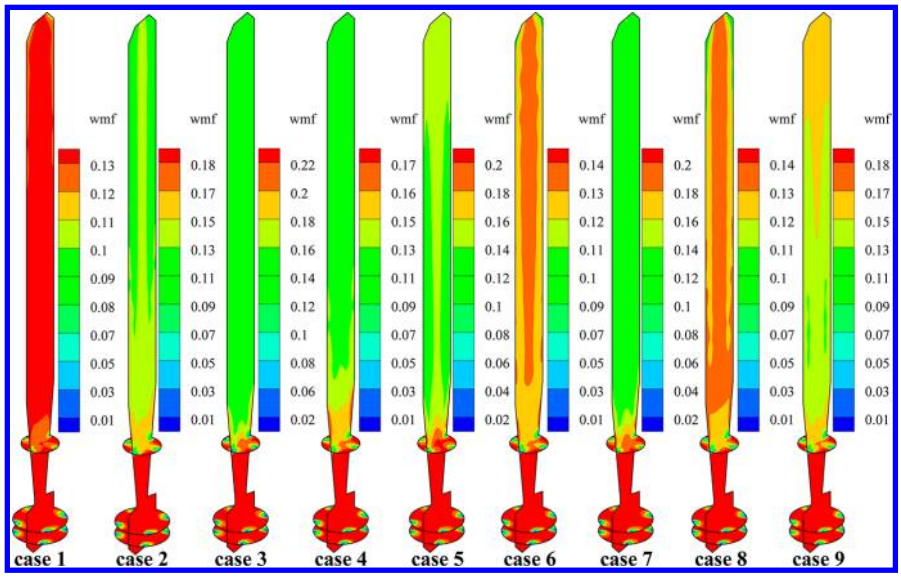

Figure 8. WMF contours for cases 1−9.

exothermic, while R2 and R3 are endothermic, when the reaction temperature is high, R2 and R3 will be promoted, while R1 will be restrained. This is not beneficial for the coal hydrogasification process. Thus, the reaction temperature should be controlled carefully.

Figure 6 shows that O_2 is consumed quickly as soon as it enters the combustor, thanks to which a high-temperature gasification agent is generated and the anaerobic hydrogasification atmosphere in the reductor is created. Thus, the gasification technology in this work is also two-stage, just like the prototype. The two-stage entrained-flow hydrogasification concept in this work is the combination of the flash hydrogasification concept, concept 1, as reported in the literature[12] and the two-stage air flow coal gasification concept, concept 2, as reported in the literature.[16] Concept 1 proposes that the coal hydrogasification agent can be generated through H_2 combustion. The direct reaction of char and hydrogen is relatively slow, but the rate of the char and steam reaction is much higher. Therefore, using this concept, the hydrogasification process can be extended greatly. Concept 2 proposes that the two-stage tangential flow coal gasifier can be used for the coal gasification. Using the two-stage gasification technology, combustion and gasification in the gasifier can be separated ingeniously and the gasification condition can also be controlled easily. In addition, the tangential flow can make the gasification agent and coal particles be well-mixed and extend the particle residence time. Another important reason is that the two-stage entrained-flow gasifier has been successfully used in the IGCC system, which is similar to the ZEC system.

The object of coal hydrogasification is to convert the carbon in coal into CH_4. Thus, MMF is a very important index to reflect the hydrogasification effect. Referring to Table 3, Figure 7 shows that MMF is almost zero in the combustor and the diffuser zones. As the hydrogasification process continues, MMF increases gradually with the height of the reductor. This is because the coal particles are injected from the diffuser nozzles. Thus, in the up-flow gasifier, the coal particles will not drop down and methane generated will not move downward either. When the feed coal enters the gasifier, it is first

dx.doi.org/10.1021/ef4013032 | *Energy Fuels* 2013, 27, 6397−6407

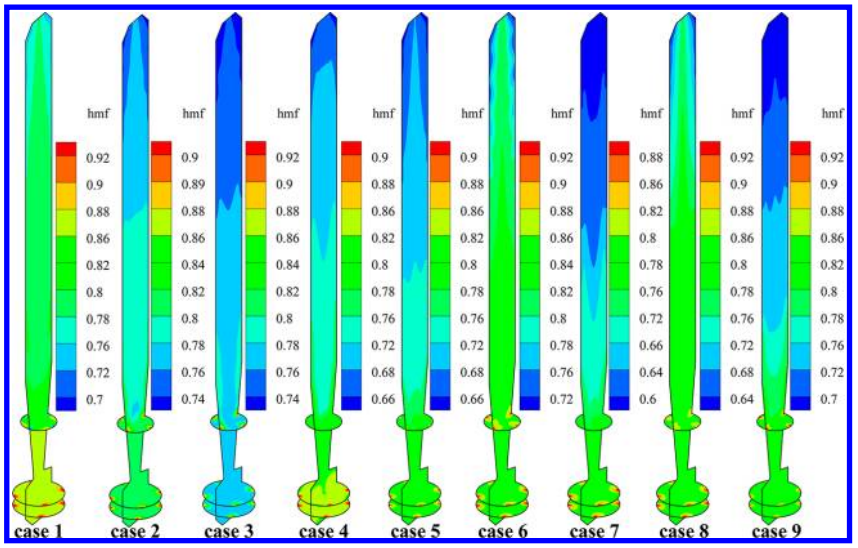

Figure 9. HMF contours for cases 1−9.

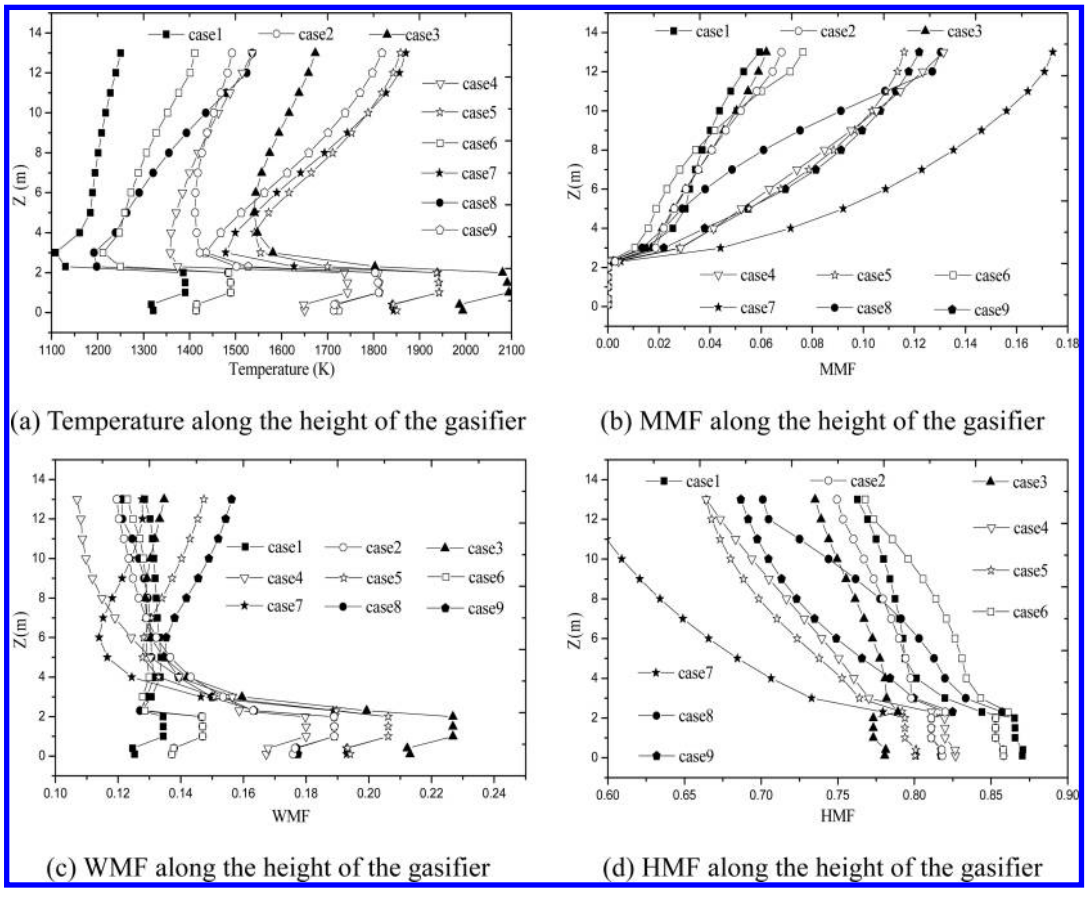

Figure 10. Comparison of the evolution histories of different parameters among cases 1−9.

pyrolyzed and part of CH_4 is extracted. Then, through the reactions between char and the gasification agent, more and more CH_4 is generated. When the reaction pressure is the same, MMF increases with the $R_{o/h}$ increment. This is because increasing $R_{o/h}$ can increase the reaction temperature. Although the hydrogasification is an exothermic reaction, when it is far from chemical equilibrium, an increasing temperature can still increase the net reaction rate. Moreover, the distribution of the CH_4 content in the top zone of the gasifier tends to be homogeneous with the increase of $R_{o/h}$. This is because the particle motion in the swirl flow is affected by the centrifugal force. When the particle is injected into the gasifier, it has a momentum component toward the center, which will gradually decrease and finally change direction under the centrifugal force. When the gasification temperature is low, the consumption of char in the gasifier will slow and the particle mass will be relatively high. Thus, the coal particles will suffer greater centrifugal force and move to the near-wall area. When the gasification temperature is high, however, the coal particles are consumed quickly and, consequently, suffer smaller

dx.doi.org/10.1021/ef4013032 | *Energy Fuels* 2013, 27, 6397−6407

centrifugal force. Thus, the distribution of the particles will be homogeneous and so is CH_4 generated by the char−gas reactions.

Figure 8 shows that the WMF in the combustor and diffuser zones is relatively high due to the H_2 combustion process. In the reductor, H_2O is diluted by N_2, H_2, and coal (the coal pyrolysis product) injected from the diffuser nozzles and WMF drops sharply. Then, many reactions about H_2O take place, but only a slight change of WMF can be detected. The technology of introducing H_2O to the coal hydrogasification is the so-called flash hydrogasification and can greatly promote the gasification process. In the original hydrogasification technology, coal is converted to CH_4 directly by R1. However, the reaction rate of R1 is relatively slow, and the char conversion rate is usually not high enough. To solve this issue, the flash hydrogasification concept is proposed in the literature.[12] They developed the flash hydrogasification technology through experiments, but the mechanism was not analyzed. In fact, when steam is added to the gasification agent, two other main reactions, R3 and the reverse reaction of R5, whose reaction rates are relatively higher, can also take place besides R1. If the two reactions are combined, R10 can be obtained. When R10 and R1 are compared, it can be seen that H_2O serves mostly like the catalyst in this concept. H_2O in the gasification product can be removed easily, and MMF can be further increased after being dried.

$$C + H_2O + 2H_2 = CH_4 + H_2O \quad \text{(R10)}$$

Figure 9 shows that HMF at the nozzle inlet is relatively high. When part of H_2 enters the combustor, it combusts with O_2 and HMF in the combustor is reduced. When part of H_2 enters the diffuser, it is diluted by the other species and the content is also reduced. Then, HMF decreases along the height of the reductor as the gasification process continues. It can also be seen from Figures 7 and 9 that the distributions of MMF and HMF are just opposite. This is because the dominant reaction in the hydrogasifier is R1; thus, the increase of MMF will lead to the decrease of HMF.

3.2. Evolution Histories of the CHG Parameters. To further understand the evolution histories of different reacting flow parameters along the height of the gasifier, the area-weighted-average values of these parameters at different heights of the gasifier are calculated and compared. The comparisons of the average temperature, MMF, HMF, and WMF along the height of the nine cases are depicted in panels a−d of Figure 10.

Figure 10a implies that the gas temperature in the combustor zone is relatively high and, in the diffuser zone, it is relatively low. Then, the gas temperature increases gradually with the height of the reductor because R1 is exothermic. Through the comparison of the cases with the same reaction pressure, it can be detected that the gas temperature is mainly controlled by $R_{o/h}$ and increases with its increment. Through the comparison of the cases with the same $R_{h/c}$, it can be found that the gas temperature is mainly controlled by $R_{o/h}$ and increases with its increment. However, when the reaction pressure is high, the effect of the reaction pressure on the gas temperature becomes significant. This is because R1 will be promoted with the p increment and more heat will be released. Through the comparison of the cases with the same $R_{o/h}$, it can be found that the reaction temperature is mainly controlled by p and increases with its increment. However, when $R_{h/c}$ is high, more hot gasification agent will be generated and the gas temperature can also be increased.

Figure 10b shows that MMF increases continually with the height of the gasifier. This is because the particle residence time increases with the gasifier height and so is the gasification extent. Through the comparison of the cases with the same reaction pressure, it can be found that MMF decreases with the $R_{h/c}$ increment. This is because when $R_{h/c}$ is high, the excessive H_2 will dilute the gasification products and MMF will be lowered. Through the comparison of the cases with the same $R_{h/c}$, it can be found that MMF increases with the $R_{o/h}$ increment. However, when the reaction pressure is high, the effect of p on MMF is also significant. Through the comparison of the cases with the same $R_{o/h}$, it can be found that MMF increases with the p increment. However, when $R_{h/c}$ is high, the excessive H_2 will dilute the gasification product and MMF will be lowered.

Figure 10c shows that WMF in the combustor is relatively high. When the gasification agent mixes with the cold gas and coal injected from the diffuser nozzles, WMF decreases sharply because of the dilution and the char−gas shift reaction. Then, WMF changes slightly along the height of the reductor. This is because H_2O serves mostly like the catalyst, as mentioned before. Through the comparison of the nine cases, WMF of cases 3, 5, 7, and 9 is found slightly increasing with the height of the reductor, while WMF of the other cases slightly decreases. This is because $R_{o/h}$ of cases 3, 5, 7, and 9 is relatively high and so is the reaction temperature in the lower part of the gasifier. Thus, the reaction of char and H_2O will be enhanced in the lower part of the gasifier, and a large amount of CO will then be generated. Then, as the gasification process continues along the reductor height, the reverse reaction of R5 will be enhanced by the abundant CO generated in the lower part. Thus, WMF will then increase with the reductor height.

Figure 10d shows that HMF decreases with the height of the gasifier because of the R1 reaction. When the reaction pressures are the same, HMF mainly depends upon $R_{o/h}$ and decreases with the $R_{o/h}$ increment. When $R_{h/c}$ is kept constant, HMF decreases with the increase of both $R_{o/h}$ and the reaction pressure. When $R_{o/h}$ is kept constant, HMF decreases with the reaction pressure. However, when $R_{h/c}$ is high, the effect of $R_{h/c}$ on HMF becomes significant.

3.3. Orthogonal Analyses. To study the effects of the three factors, p, $R_{h/c}$, and $R_{o/h}$ on the gasification evaluation indexes, CCR, MMF, and CGE, the orthogonal analysis method is used. The area-weighted-average values of CCR, MMF, and CGE at the outlet of the gasifier are listed in Table 6 for the nine cases.

From Table 6, it can be seen that the maximum CCR (99.31%) is obtained from case 9, the maximum MMF

Table 6. Area-Weighted-Average CCR, MMF, and CGE at the Outlet of the Gasifier

case number	CCR (%)	MMF (%)	CGE (%)
1	12.49	5.94	74.3
2	72.63	6.80	82.5
3	95.76	6.21	82.2
4	77.27	13.13	77.5
5	99.15	11.61	78.9
6	66.51	7.64	82.7
7	96.78	17.42	76.4
8	84.62	13.03	80.4
9	99.31	12.19	80.0

dx.doi.org/10.1021/ef4013032 | Energy Fuels 2013, 27, 6397−6407

(17.42%) is obtained from case 7, and the maximum CGE (82.7%) is obtained from case 6. To find the sensitivity of these parameters to the operating conditions and find the optimum combination of the operating conditions, detailed calculation analysis is performed, and the results are listed in Table 7.

Table 7. Orthogonal Analysis Table

		p	$R_{h/c}$	$R_{o/h}$
CCR	k_1	180.88	186.54	163.62
	k_2	242.93	256.40	249.21
	k_3	280.71	261.58	291.69
	$\bar{k}_1$	60.29	62.18	54.54
	$\bar{k}_2$	80.98	85.47	83.07
	$\bar{k}_3$	93.57	87.19	97.23
	R	33.28	25.01	42.69
MMF	k_1	18.95	36.49	26.61
	k_2	32.38	31.44	32.12
	k_3	42.64	26.04	35.24
	$\bar{k}_1$	6.32	12.16	8.87
	$\bar{k}_2$	10.79	10.48	10.71
	$\bar{k}_3$	14.21	8.68	11.75
	R	7.90	3.48	2.88
CGE	k_1	239	228	237
	k_2	239	242	240
	k_3	237	245	237
	$\bar{k}_1$	80	76	79
	$\bar{k}_2$	80	81	80
	$\bar{k}_3$	79	82	79
	R	1	6	1

k_i, in Table 7, denotes the sum of the index values corresponding to the ith level of each of the factors. $\bar{k}_i$, in Table 7, denotes the algebraic average of the index values corresponding to the ith level of each of the factors. R is called the "range" mathematically and denotes the difference of the maximum and minimum $\bar{k}_i$. When R values in Table 7 are compared, the sensitivity of the indexes to each of the factors can be found. Ranked in descending order, the effect degree of the factors on CCR is $R_{o/h} > p > R_{h/c}$; the effect degree of the factors on MMF is $p > R_{h/c} > R_{o/h}$; and the effect degree of the factors on CGE is $R_{h/c} > R_{o/h} = p$. When k_i values in Table 7 are compared, the optimum combination of the factors for CCR should be p = 7 MPa, $R_{h/c}$ = 0.7, and $R_{o/h}$ = 1.5; the optimum combination of the factors for MMF should be p = 7 MPa, $R_{h/c}$ = 0.3, and $R_{o/h}$ = 1.5; and the optimum combination of the factors for CGE should be p = 3 MPa (p = 5 MPa), $R_{h/c}$ = 0.7, and $R_{o/h}$ = 1.25.

It is expected that the values of CCR, MMF, and CGE should be as high as possible. Unfortunately, no combination of the operating conditions can make these three evaluation indexes reach their highest values simultaneously. Thus, a comprehensive optimum combination of the operating conditions should be considered. First, it can be seen from the orthogonal analysis that the optimum reaction pressure for CCR and MMF is 7 MPa, while the best reaction pressure for CGE is 3 or 5 MPa. This is because increasing the reaction pressure can promote the char methanation reaction, R1, in Table 2 because of the principle of Le Chatelier.[23] Thus, CCR and MMF will increase with the increment of p. Because the char methanation reaction is exothermic, more heat will be released at higher reaction pressure and become the sensible heat of the gasification product. Thus, CGE, which does not include the sensible heat, will decrease with the increment of p. However, either in the IGCC system or in the ZEC system, the hot gas from the gasifier enters the following components directly without cooling and the sensible heat can be used. Therefore, p should be set to a relatively high value, even though CGE might be lowered in that case. Second, it can be seen from the orthogonal analysis that the optimum $R_{h/c}$ for CCR and CGE is 0.7, while the optimum $R_{h/c}$ for MMF is 0.3. This is because increasing $R_{h/c}$ can increase the partial pressure of H_2 in the hydrogasifier and then promote the char methanation reaction. When $R_{h/c}$ is high, the mole fractions of H_2 in the inlet gasification agent and the gasification product will be high and the chemical energy of H_2 will account for a large proportion; thus, CGE will be increased. When $R_{h/c}$ is large enough, CGE can be close to 1, which is however meaningless. From the char methanation reaction, R1, it can be seen that 1 g of H_2 can react with 3 g of C. In the actual CHG process, the mass fraction of carbon in char is not 100% and C can also react with other species, such as H_2O and CO_2. High $R_{h/c}$ can promote the char methanation reaction and increase CGE, but excessive H_2 can also dilute the gasification product. In addition, from the orthogonal analysis, the effect of $R_{h/c}$ on CCR is found the slightest. Thus, it is proposed to set $R_{h/c}$ with 0.3. Third, it is found from the orthogonal analysis that the optimum value of $R_{o/h}$ for CCR and MMF is 1.5 and the optimum value of $R_{o/h}$ for CGE is 1.25. This is because increasing $R_{o/h}$ can increase the temperature and the H_2O content in the gasification agent, which is beneficial to the char conversion and can also promote the char methanation reaction because H_2O serves mostly like the catalyst in the CHG process. Because CGE does not include the sensible heat in the gasification product, increasing $R_{o/h}$ can lower the value of CGE to a certain extent. However, it does not matter because the sensible heat can be used in the ZEC system. Thus, it is proposed to set 1.5 to $R_{o/h}$. After the comprehensive analyses, it is proposed that the optimum combination of the operating conditions should be p = 7 MPa, $R_{h/c}$ = 0.3, and $R_{o/h}$ = 1.5. With this parameter combination, CCR can be 96.78%, MMF can be 17.42%, and CGE can reach 76.4%.

4. CONCLUSION

To seek the hydrogasification characteristics of a two-stage gasifier, which is originally developed for coal gasification with air in the IGCC system that is similar to the ZEC system, nine cases with different operating conditions are designed with the orthogonal method and the corresponding three-dimensional (3D) numerical simulations are performed with the model setup in our former work. The fields of the key parameters of the reacting flow in the gasifier are first analyzed. The evolution histories of the parameters along the height of the gasifer are then compared for the nine cases. The sensitivities of CCR, MMF, and CGE to different operating conditions are finally investigated, and the optimal combination of the operating conditions is proposed. With all of the work performed, meaningful conclusions are drawn and summarized as follows: (1) With the combination of the flash hydrogasification concept and the two-stage entrained-flow-bed concept, the original two-stage entrained-flow gasifier developed in Japan can be reformed for coal hydrogasification and performs well with proper operating conditions. (2) Counter flow in the gasifier is generated because of the tangential injections from the combustor nozzles and is beneficial to the carbon conversion. The gas temperature in the gasifier mainly depends

dx.doi.org/10.1021/ef4013032 | Energy Fuels 2013, 27, 6397−6407

upon $R_{o/h}$ and will increase with the height of the reductor. O_2 is consumed quickly when it enters the combustor, and the anaerobic atmosphere in the reductor is created. MMF increases gradually with the height of the reductor, and the distribution of CH_4 in the top zone of the reductor tends to be homogeneous with the increase of $R_{o/h}$. The introduction of H_2O can promote the gasification process, and it works mostly like the catalyst. HMF decreases with the height of the gasifier as the gasification process continues, and its distribution is opposite to that of MMF. (3) The temperature distribution along the height of the gasifier mainly depends upon $R_{o/h}$. However, when p and $R_{h/c}$ are high, their effects on the gas temperature are also significant. The MMF distribution along the height of the gasifier mainly depends upon $R_{o/h}$. However, when p is high, the effect of p on MMF is also significant. When $R_{h/c}$ is high, excessive H_2 will dilute the gasification products and MMF will be lowered. WMF distribution along the symmetry axis slightly increases with the height of the gasifier if the gasification temperature is high; otherwise, it will slightly decrease. HMF distribution along the symmetry axis decreases with the height of the gasifier, especially when $R_{o/h}$ and p are high. (4) Ranked in descending order, the effect degree of the factors on CCR is $R_{o/h} > p > R_{h/c}$; the effect degree of the factors on MMF is $p > R_{h/c} > R_{o/h}$; and the effect degree of the factors on CGE is $R_{h/c} > R_{o/h} = p$. The optimum combination of the factors for CCR should be p = 7 MPa, $R_{h/c}$ = 0.7, and $R_{o/h}$ = 1.5; the optimum combination of the factors for MMF should be p = 7 MPa, $R_{h/c}$ = 0.3, and $R_{o/h}$ = 1.5; and the optimum combination of the factors for CGE should be p = 3 MPa (p = 5 MPa), $R_{h/c}$ = 0.7, and $R_{o/h}$ = 1.25. The synthetically optimal combination of the operating condition is p = 7 MPa, $R_{h/c}$ = 0.3, and $R_{o/h}$ = 1.5. With this combination, CCR can be 96.78%, MMF can be 17.42%, and CGE can reach 76.4%.

AUTHOR INFORMATION

Corresponding Author

*Telephone: +86-10-5168-8542. Fax: +86-10-5168-8404. E-mail: hebs@bjtu.edu.cn.

Notes

The authors declare no competing financial interest.

ACKNOWLEDGMENTS

The authors gratefully acknowledge the financial support from the National Natural Science Foundation of China (NSFC, 50876008 and 51176009) and the Fundamental Research Funds for the Central Universities (2013YJS078) for this work.

NOMENCLATURE

CCR = carbon conversion rate
CGE = cold gas efficiency
CHG = coal hydrogasification
CRPSC−PC = combined random pore and shrinking core model with pressure correction
CSR = cross-section of the reductor
DO = discrete ordinates
DPM = discrete phase model
EDC = eddy-dissipation concept
HMF = hydrogen (H_2) mole fraction
IGCC = integrated gasification combined cycle
ISAT = *in situ* adaptive tabulation
MMF = methane (CH_4) mole fraction
OMF = oxygen (O_2) mole fraction
PRT = particle residence time
RKE = realizable $k-\varepsilon$
SR = swirl ratio
WMF = water (H_2O) mole fraction
WSGGM = weighted-sum-of-gray-gases model
ZEC = zero emission coal

REFERENCES

(1) Mondal, P.; Dang, G. S.; Garg, M. O. Syngas production through gasification and cleanup for downstream applications—Recent developments. *Fuel Process. Technol.* **2011**, *92*, 1395−1410.

(2) Xu, S. S.; Zhang, D. L.; Ren, Y. Q. *Large Scale Coal Gasificatioin Technology*; Chemical Industry Press: Beijing, China, 2008 (in Chinese).

(3) Chandra, D.; Elsworth, D.; VanEssendelft, D. Mechanical and transport characteristics of coal−biomass mixtures for advanced IGCC systems. *Energy Fuels* **2012**, *26* (9), 5729−5739.

(4) Ziock, H. J.; Lackner, K. S.; Harrison, D. P. *Zero Emission Coal Power, A New Concept*; Los Alamos National Laboratory: Los Alamos, NM, 2001; Contract LA-UR-01-2214, http://www.netl.doe.gov/publications/proceedings/01/carbon_seq/2b2.pdf.

(5) He, B. S.; Li, M. Y.; Wang, X.; Zhu, L.; Wang, L. L.; Xue, J. W.; Chen, Z. X. Chemical kinetics-based analysis for utilities of ZEC power generation system. *Int. J. Hydrogen Energy* **2008**, *33*, 4673−4680.

(6) Yan, L. B.; He, B. S.; Ma, L. L.; Pei, X. H.; Wang, C. J.; Li, X. S. Integrated characteristics and performance of zero emission coal system. *Int. J. Hydrogen Energy* **2012**, *37*, 9669−9676.

(7) Hotchkiss, R. Coal gasification technology. *Proc. Inst. Mech. Eng., Part A* **2003**, *217*, 27−32.

(8) Yan, L.; He, B.; Pei, X.; Wang, C.; Li, X.; Duan, Z. Kinetic models for coal hydrogasification and analyses of hydrogasification characteristics in entrained flow gasifiers. *Energy Fuels* **2013**, DOI: 10.1021/ef401302b.

(9) Lee, S. H.; Lee, J. G.; Kim, J. H.; Choi, Y. C. Hydrogasification characteristics of bituminous coals in an entrained-flow hydrogasifiers. *Fuel* **2006**, *85*, 803−806.

(10) Xu, W. C.; Matsuoka, K.; Akiho, H.; Kumagai, M.; Tomita, A. High pressure hydropysolysis of coals by using a continuous free-fall reactor. *Fuel* **2003**, *82*, 677−685.

(11) Zhang, A.; Kaiho, M.; Yasuda, H.; Zabat, M.; Nakano, K.; Yamada, O. Fundamental studies on hydrogasification of Taiheiyou coal. *Energy* **2005**, *30*, 2243−2250.

(12) Falk, A. Y.; Schuman, M. D.; Kahn, D. R. *Advancement of Flash Hydrogasification: Task VIII—Performance Testing*; Morgantown Energy Technology Center: Morgantown, WV, 1986; Contract DE-AC21-78ET10328, http://www.osti.gov/bridge/purl.cover.jsp?purl=/5377768-SKAxm4/5377768.pdf.

(13) Friedman, J. *Development of a Single-Stage, Entrained-Flow, Short-Residence-Time Hydrogasifier*; National Technical Information Service: Alexandria, VA, 1979; Contract FE-2518-24.

(14) Chen, C. X.; Horio, M.; Kojima, T. Numerical simulation of entrained flow coal gasifiers. Part I: Modeling of coal gasification in an entrained flow gasifier. *Chem. Eng. Sci.* **2000**, *55*, 3861−3874.

(15) Chen, C. X.; Horio, M.; Kojima, T. Use of numerical modeling in the design and scale-up of entrained flow coal gasifers. *Fuel* **2001**, *80*, 1513−1523.

(16) Chen, C. X.; Takahiro, M.; Kajima, H.; Horio, M.; Kojima, T. On the scaling-up of a two-stage air blown entrained flow coal gasifier. *Can. J. Chem. Eng.* **1999**, *77*, 745−750.

(17) Yan, L. B.; He, B. S.; Pei, X. H.; Li, X. S.; Wang, C. J.; Liang, H. X. Kinetic model and prediction for coal hydrogasification. *Int. J. Hydrogen Energy* **2013**, *38* (11), 4513−4523.

(18) Shih, T. H.; Liou, W. W.; Shabbir, A.; Yang, Z.; Zhu, J. A new $k-\varepsilon$ eddy viscosity model for high Reynolds number turbulent flows—Model development and validation. *Comput. Fluids* **1995**, *24*, 227−238.

(19) Siegel, R.; Howell, J. R. *Thermal Radiation Heat Transfer*; Hemisphere Publishing Corporation: Washington, D.C., 1992.

(20) Smith, T. F.; Shen, Z. F.; Friedman, J. N. Evaluation of coefficients for the weighted sum of gray gases model. *J. Heat Transfer* **1982**, *104*, 602−608.
(21) Magnussen, B. F. On the structure of turbulence and a generalized eddy dissipation concept for chemical reaction in turbulent flow. Proceedings of the 19th American Institute of Aeronautics and Astronautics (AIAA) Meeting; St. Louis, MO, Jan 12−15, 1981; AIAA-1981-0042, http://folk.ntnu.no/ivarse/edc/EDC1981.pdf.
(22) Pope, S. B. Computationally efficient implementation of combustion chemistry using in-situ adaptive tabulation. *Combust. Theor. Model* **1997**, *1*, 41−63.
(23) George, W. R. *Chemical Reactions and Chemical Reactors*; John Wiley and Sons, Inc.: Hoboken, NJ, 2009.